buildings

MDPI

Article

Enhancing Construction Efficiency and Structural Integrity of Ambient-Cured UHPC Incorporating Sulfoaluminate Cement Through Liquid Superplasticizer Optimization

Anwar Saleem, Ergang Xiong *, Mabor Achol Samuel and Mahmood Haris

School of Civil Engineering, Chang'an University, Xi'an 710061, China; anwarsaleem@chd.edu.cn (A.S.); maborachol@chd.edu.cn (M.A.S.); harismahmood@chd.edu.cn (M.H.)
* Correspondence: xerg@chd.edu.cn

Abstract

The addition of sulfoaluminate cement (SAC) to ultra-high-performance concrete (UHPC) enables sustainable high-speed construction due to the high 7-day strength without thermal curing. The fast hydration of SAC, however, endangers the admixture efficacy, which may compromise the structural integrity of the infrastructure components. This study investigates the effect of the physical form of polycarboxylate ether (PCE) superplasticizers on the performance of UHPC with the incorporation of SAC in ambient conditions. A paired experimental design of 32 mixtures compared liquid superplasticizers (LSPs) and powder superplasticizers (PSPs) in various binder compositions (OPC/SAC of 1/4–4/1) and water-to-binder ratios (0.18–0.21) at a constant dosage of admixtures of 1% except where w/b 0.18 (1.5% superplasticizers and 1% retarders were used). Findings indicate that LSPs enhance workability and compressive strength by 45% and 10.03%, respectively. The underlying mechanism is explained by comprehensive microstructural characterization through the use of Scanning Electron Microscopy (SEM), X-ray Diffraction (XRD) and Fourier Transform Infrared (FTIR) spectroscopy. SEM study showed a 23% decrease in porosity, and XRD patterns showed the increased formation of amorphous C-S-H gel for LSPs. The higher levels of Al^{3+} incorporated into the gel structure (C-A-S-H) of the liquid forms was also verified by FTIR spectra. Mechanically, the research reveals one of the kinetic mismatches, where the rate of SAC hydration is greater than the rate of powder dissolution, which leads to a failure to fully disperse and shear-controlled failures. LSPs, in contrast, make it possible to disperse particles immediately, so the matrices become more dense and shift to axial failure. These results provide practical guidelines to infrastructure engineers to use liquid superplasticizer in SAC-based systems in order to achieve sustainability and reliability in terms of performance in precast and fast-track construction projects.

Keywords: ultra-high-performance concrete (UHPC); sulfoaluminate cement (SAC); liquid superplasticizer; precast construction; structural integrity

Check for updates

Academic Editor: Antonio Caggiano

Received: 28 February 2026
Revised: 26 April 2026
Accepted: 27 April 2026
Published: 26 May 2026

Copyright: © 2026 by the authors. Licensee MDPI, Basel, Switzerland. This article is an open access article distributed under the terms and conditions of the Creative Commons Attribution (CC BY) license.

1. Introduction

Ultra-high-performance concrete (UHPC) was introduced by Richard and Cheyrezy [1,2]. UHPC marks a notable advancement in concrete technology, distinguished by its ultra-low water-to-binder ratio, dense microstructure, and exceptional mechanical properties [3–5]. Unlike conventional concrete, UHPC is crafted with an optimized particle packing design, eliminating coarse aggregates and incorporating supplementary cementitious materials (SCMs)

such as silica fume and fly ash [6–8]. These features make UHPC an ideal choice for demanding structural applications, including long-span bridges, precast facade elements, and blast-resistant infrastructures [9,10]. It is acknowledged that while UHPC is frequently characterized by compressive strengths exceeding 150 MPa [11], such values typically require heat curing or autoclaving. In this study, the term UHPC is adopted based on the composite design philosophy, specifically the ultra-low water-to-binder ratio (0.18–0.21), optimized particle packing, and 3% steel fiber reinforcement [12], rather than strength alone. This classification aligns with the recent literature recognizing ambient-cured UHPC systems achieving 100–120 MPa as valid variants when design criteria are prioritized [13–15]. Accordingly, the material is explicitly referred to as "ambient-cured UHPC" throughout to ensure terminological precision.

Superplasticizers are crucial in UHPC mixtures, facilitating high flowability at low water-to-binder ratios while preserving mechanical performance [16,17]. Since the introduction of applications in the 1930s, they have been used as critical chemical admixtures for modern concrete [18]. Different types of superplasticizers, such as sulfonated melamine [19], carbon nanotubes [20], formaldehyde [21], sulfonated naphthalene [22] and polycarboxylate ethers (PCEs) [23], are commonly employed, each with distinct dispersion mechanisms and efficiency levels. Recent advances in PCE technology have emphasized the critical role of molecular structure, particularly functional groups such as carboxyl, ester, siloxane, phosphate, and sulfonic groups, in governing electrostatic repulsion, steric hindrance, and adsorption behavior within cementitious matrices [17,24–26]. Additionally, PCE significantly influences early-age hydration dynamics and structural build-up by modifying colloidal interactions and the formation of hydration products like C-S-H and ettringite [17,27,28]. The careful selection and dosage of superplasticizers are therefore essential to optimize rheology, setting time, and the ultimate performance of UHPC [23,29]. PCE-based superplasticizers, developed as the new generation in 1980s, can achieve up to 40% water reduction [30]. In practical applications, these superplasticizers are available commercially in two primary forms, powder and liquid, each with unique characteristics, benefits, and limitations [31]. Powder superplasticizers (PSPs) are often favored in dry-mix UHPC formulations and pre-bagged concrete products due to their extended shelf life, ease of storage, and lower transportation costs [32]. They also provide flexibility for dry blending with other powder components during pre-mixing [33]. Conversely, liquid superplasticizers (LSPs) are more frequently used in ready-mix and in situ concrete applications because of their ease of dosing, rapid dispersion, and immediate effectiveness in altering mix rheology [18]. Powdered SPs, typically derived from sulfonated melamine formaldehyde (SMF) or naphthalene sulfonate formaldehyde (NSF), offer logistical benefits such as longer shelf life and easier integration into dry-mix systems [34]. The retarders are also very important in UHPC, as they help to extend the setting time, SAC-based UHPC even setting faster, but the dosage should be selected carefully, as increasing the amount inversely affects the mechanical properties [35]. The optimized dosage is recommended at 0.5–1% by volume [16].

Superplasticizers have a significant impact on the workability of concrete, which encompasses the ease of mixing, placing, compacting and finishing the concrete mixture [36]. In UHPC, workability is especially crucial due to the fineness of the particles and the absence of coarse aggregates, which can increase internal friction [37]. Ensuring proper workability is essential for achieving homogeneous mixing, complete compaction, and defect-free casting, all of which enhance the structural integrity and long-term durability of the hardened product. The type of superplasticizer influences not only the initial slump or flow of the mix but also its thixotropic behavior and the retention of workability over time [38–41]. Notably, powder superplasticizers might require more mixing time for full activation and dispersion, whereas liquid versions act more quickly but may experience a

faster slump loss over time. In structure applications, the accelerated kinetics of SAC (initial set of 20 min) impose strict boundary conditions on the mixing and placement energy. Inadequate dispersion kinetics relative to hydration rates can compromise consolidation efficiency and extend formwork retention times, directly impacting project throughput.

The impact of superplasticizers on the compressive strength of UHPC is equally significant, especially at 7 days [42]. Early-age strength is crucial for fast-track construction schedules, precast element de-molding, and performance verification [14]. Superplasticizers reduce water demand while maintaining or enhancing flowability, resulting in a denser, less porous microstructure that directly boosts compressive strength [43]. However, the form of the superplasticizer, whether powder or liquid, can affect the kinetics of cement hydration, the dispersion of cement particles, and the degree of microstructural refinement, thereby influencing strength gain. Additionally, powder-based admixtures may offer delayed release mechanisms, potentially altering hydration profiles and the 7-day strength development compared to their liquid counterparts.

Most existing studies concentrate either on the rheology of pastes or on standard concretes with higher w/b ratios, which do not accurately represent the extreme conditions found in UHPC formulations [30,44]. In UHPC, the high binder content, fine particles (e.g., nano-silica), and dense packing structure create a complex environment where the efficiency of superplasticizers is more sensitive to dosage, chemical structure, and dispersion kinetics [45,46]. The majority of the available literature focuses on the effects of chemical composition and dosage, with limited exploration of how physical form influences key properties like flowability and 7-day strength in high-performance applications [47]. Additionally, a significant portion of existing UHPC literature relies on a single form of superplasticizer [20,48], often without evaluating alternatives, which may restrict the broader applicability of their findings. Crucially, the interaction between superplasticizer physical form and cement chemistry remains underexplored, particularly for rapid-setting binders like SAC. Unlike OPC, SAC exhibits accelerated hydration kinetics, with initial setting times as low as 20 min. This raises a potential kinetic competition; while the bulk dissolution of PCE can be rapid under high-shear mixing, the time required for polymer chain extension and adsorption onto cementitious surfaces in ultra-low w/b systems may compete with the accelerated ettringite formation in SAC. It is hypothesized that if effective dispersion and steric stabilization are not achieved before matrix stiffening, microstructural defects may arise that are not typically observed in OPC systems.

Consequently, this study addresses two critical gaps. Scientifically, the kinetic competition between accelerated SAC hydration rates (initial set of 20 min) and powder superplasticizer dissolution kinetics remains unquantified in ultra-low w/b systems. Practically, this mismatch poses risks to construction efficiency (workability retention) and structural integrity (strength consistency) in precast and fast-track projects. To resolve these issues, this research aims to: (1) quantify the effect of PCE physical form on rheology and compressive strength at w/b ratios of 0.18–0.21; (2) elucidate the microstructural mechanisms via SEM, XRD, and FTIR; and (3) establish technical guidelines for admixture selection in SAC-based UHPC applications for both precast and cast-in-place application.

2. Materials and Methodology

In this study, all constituent materials are sourced domestically within China except powder SPs. The primary binder system comprises sulphoaluminate cement (SAC) and ordinary Portland cement (OPC), complemented by silica fume (SF) and fly ash (FA) as supplementary cementitious materials. Quartz sand (QS) is employed as the fine aggregate, while steel fibers (sf) are incorporated to enhance the mechanical properties and toughness of the UHPC. Chemical admixtures include a retarder (Ret) to control the setting time

and SPs to ensure high flowability at a low water-to-binder ratio. Since the focus of this investigation is on evaluating the influence of different types of superplasticizers, the proportions of all other mix constituents are held constant. This approach ensures that any variation in the fresh and hardened properties of UHPC can be attributed solely to the type and characteristics of the SPs employed.

2.1. Cementitious Materials

In the present investigation, the incorporated cementitious constituents comprise SAC, OPC, SF, and FA, depicted in Figure 1. The interaction between SAC and OPC increases Ca^{2+} and Al^{3+} ions, promoting rapid C–S–H and C–A–S–H formation and improving the 7-day strength stability. All binder materials are procured from CONCH Co., Ltd., Shaanxi, China, ensuring consistent supply and quality. The physical and chemical properties of primary binders are summarized in Table 1. The physical and chemical properties of all raw materials are obtained directly from supplier specifications and were not independently measured in this study. The combined use of supplementary cementitious materials such as SF and FA aims to enhance the pozzolanic reaction, refine the pore structure, and contribute to the long-term durability and strength development of the ultra-high-performance concrete (UHPC) mixtures. Table 2 outlines the physical properties and chemical composition of supplementary cementitious materials.



(a) OPC (b) SAC (c) FA (d) SF

Figure 1. Binder materials.

Table 1. Physical and chemical properties of primary binders.

Physical Properties			Chemical Properties		
Properties	**OPC**	**SAC**	**Composition**	**OPC (%)**	**SAC (%)**
Flexural Strength (3d)	4.0 MPa	5.9 MPa	Al_2O_3	3–8	28.3
Flexural Strength (7d)	4.5 MPa	6.9 MPa	CaO	60–67	42.7
Compressive Strength (3d)	31.9 MPa	33.9 MPa	SO_3	≤3.5	10.4
Compressive Strength (7d)	42.5 MPa	45.5 MPa	SiO_2	17–25	10.50
Initial Setting Time	45 min	20 min	Fe_2O_3	0.5–6	2.3
Final Setting Time	600 min	40 min	MgO	5	1.22
Specific Surface Area	360 m^2/kg	425 m^2/kg	TiO_2	-	1.5
Sieve Residue (80 μm)	1.87%	-	$Na_2O + K_2O$	≤0.6–1	-

Table 2. Physical and chemical properties of supplementary cementitious materials.

Physical Properties			Chemical Properties		
Properties	**SF**	**FA**	**Composition**	**SF (%)**	**FA (%)**
Appearance	Fine, gray powder	Fine, gray powder	SiO_2	95.03	60
Particle Size	0.5 μm	100 μm	Loss	1.96	-
Specific Surface Area	20,880 m^2/kg	600 m^2/kg	Al_2O_3	0.38	20
Density	2.2–2.3 g/cm^3	2.6 g/cm^3	CaO	0.59	6
Color	Grey to white	Dark grey	MgO	0.54	2.5
Bulk Density (kg/m^3)	400	1200	Fe_2O_3	0.08	10
Particle Shape	Spherical	Spherical	R_2O	-	0.53

2.2. Fine Aggregates

Fine aggregates such as quartz sand are also an important factor, and the purity of quartz sand plays an important role in the compressive strength of UHPC as shown in Figure 2. As required, the quartz sand selected for this research is gradation based. In the present investigation, fine aggregates with consistent classification and a specific gravity of 2.65 are used, and the gradation of filler materials is shown in Figure 3. A sieve analysis of the filler materials is shown in Table 3.



Figure 2. Different grades of quartz sand classified by sieve mesh size ranges.

Table 3. Gradation Data of Quartz Sand.

Sieve (mesh)	Size (mm)	Mass Retained (g)	% Retained	Cum. % Retained	% Passing
20	0.850	282.5	33.3	33.3	66.7
40	0.425	259.0	30.6	63.9	36.1
70	0.212	165.0	19.5	83.4	16.6
120	0.125	141.0	16.6	100.0	0.0
Pan	0.000	0.0	0.0	100.0	0.0

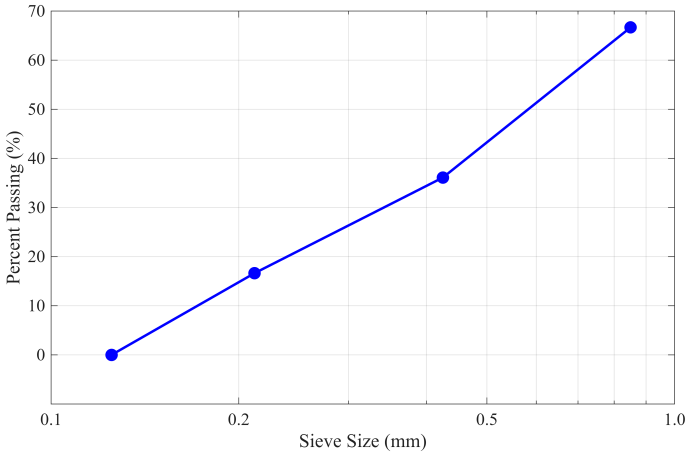


Figure 3. Gradation curve of quartz sand.

The quartz sand exhibits exceptionally high purity with 99.51% silica (SiO_2) content. The impurity levels are minimal, with the most significant being calcium oxide (CaO) at 0.33.

2.3. Admixtures

UHPC needs admixtures because of highly reactive binding materials. In this research work, a citric-acid-based organic retarder (Henan Hoshen Industrial Co., Ltd., Nanyang, China) is used to control the rapid setting of SAC. Citric acid temporarily complexes with Ca^{2+} ions, slowing C_4A_3 dissolution and ettringite formation, which effectively extends the setting time and ensures uniform mixing without compromising early strength. Superplasticizers are also very important and used in two forms, one as powder and the other as liquid.

Although the two PCEs differ in physical form, the active polymeric component is chemically identical: both are comb-type polycarboxylate ether copolymers with the same functional groups (–COOH, –SO3H, –OH), molecular weight distribution, and grafting density. This experimental design ensures that any observed performance differences arise solely from the physical state (pre-dissolved vs. solid) and its influence on dissolution kinetics and dispersion behavior, rather than from chemical composition. Prior to use, the powder PCE is visually inspected to remove any insoluble inorganic particles. This ensures that only the active polymer contributes to dispersion, preventing interference with UHPC rheology and maintaining consistent workability and early-age performance. The powder and liquid superplasticizers are procured from Shaanxi Feike new Materials Technology Co., Ltd., Yuncheng, China, where liquid superplasticizers have 40% water content and 60% solid content. The properties of both liquid and powder superplasticizers are given in Table 4. All these admixtures are shown in Figure 4.



Figure 4. Liquid Superplasticizers(LSP), Powder Superplasticizers(PSP) and Retarders(Ret).

Table 4. Chemical properties of superplasticizers (SPs) used in UHPC.

Property	**General PCE Superplasticizers**	**MasterGlenium® ACE 30 (Powdered PCE, Shaanxi Feike New Materials Technology Co., Ltd. Shaanxi, China)**
Appearance	Liquid: Clear or slightly cloudy	White to off-white free-flowing powder
Functional Groups	–COOH, –SO_3H, –OH	–COOH, –SO_3H, –OH
Solid Content	60%	100% (dry powder)
pH Value	6.0	6.0 (1% solution)
Chloride Content (Cl^-)	≤0.1%	<0.1%
Solubility	Fully water-soluble	Fully water-soluble
Water-Reducing Rate	≥27%	High water reduction
Typical Dosage by weight of binder	0.5–2.0%	0.5–0.2% by weight of binder
Compatibility	Optimized for silica fume and microfillers	Optimized for UHPC mix designs

2.4. Steel Fibers

Steel fibers are small, high-strength reinforcements added to UHPC to improve its strength, toughness, and crack resistance. They bridge microcracks, enhancing durability and load-bearing capacity, making UHPC ideal for demanding applications like bridges and seismic-resistant structures. In the present research, steel fibers are added at 3% by volume of the UHPC to enhance the compressive strength. The physical properties of steel fibers used in this research are shown in Table 5.

Table 5. Physical properties of steel fibers.

Property	Value/Range	Property	Value/Range
Length	13 mm	Diameter	0.2 mm
Aspect Ratio	65	Shape	Straight
Tensile Strength	2000 MPa	Density	7.8 g/cm^3
Elastic modulus	210 GPa	Durability	stainless steel

2.5. Experimental Program

The experimental work is designed to quantify the influence of the physical form of a PCE superplasticizer on the fresh and hardened properties of SAC-based UHPC. The program combines mix design, preparation and testing procedures into a single, controlled framework. The total binder content (≈1240 kg/m^3) is intentionally held constant across all mixtures to isolate superplasticizer form effects while maintaining adequate paste volume and workability at ultra-low w/b ratios. Each unique mix formulation is duplicated, once with a liquid superplasticizer and once with its powdered counterpart, resulting in a paired comparison scheme with total 16 pairs. For consistency and direct comparability, the SP dosage is standardized as a weight percentage of the total binder content. LSPs are incorporated into odd-numbered specimen batches (e.g., Mix 59, 61, 63. . .), whereas the equivalent mixes with PSPs are assigned to even-numbered batches (e.g., Mix 60, 62, 64. . .). This design allows for rigorous statistical comparison of the performance metrics between the two SP forms under identical mix conditions. The percentages of these materials are depicted in Figure 5. The exact amount of all the materials in specific samples is shown in Table A1, whereas all the values are reported by weight. For each mix design, two separate batches are prepared according to the Figure 6 showing full mixing details with both SPs (with the same mixing process for both SPs) to ensure sufficient material for all required tests: one batch for slump flow and two batches for the hardened property (3.0 kg total mass) for casting compressive strength specimens. The hardened-property batches are used to cast six 70 mm cubes (three replicates each for 7-day and 28-day testing). For microstructure analysis, the specimens are well ground and then passed through mesh 200 for FTIR and XRD, while for SEM the samples are collected after crushing the specimens under a compressive test, where the small inner portion of the samples are collected.These samples are carefully extracted, oven-dried at 40 °C for 24 h, and sputter-coated with gold layer prior to SEM imaging to ensure electrical conductivity and prevent charge accumulation.

Quantitative porosity analysis was performed using Python 3.10 (Google Colab) with OpenCV and scikit-image. SEM micrographs are converted to grayscale, contrast-enhanced using CLAHE (clip limit = 2.0, tile size = 8 × 8), and smoothed with a 5 × 5 Gaussian filter. Pore segmentation employs Otsu's adaptive thresholding with a conservative scaling factor (0.5× the Otsu value) to prevent overestimation, followed by morphological opening/closing and the removal of features <30 pixels. The resulting 2D pore area fraction is used as a relative indicator of porosity. While absolute 3D porosity is not cross-validated with mercury intrusion porosimetry (MIP), identical acquisition parameters and standardized preprocessing ensure reliable comparative assessment between the LSP and PSP specimens.

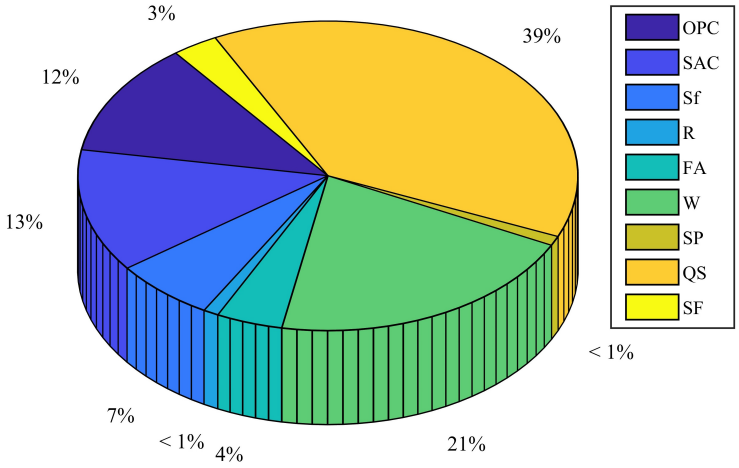


Figure 5. Material percentage for trial mixes.

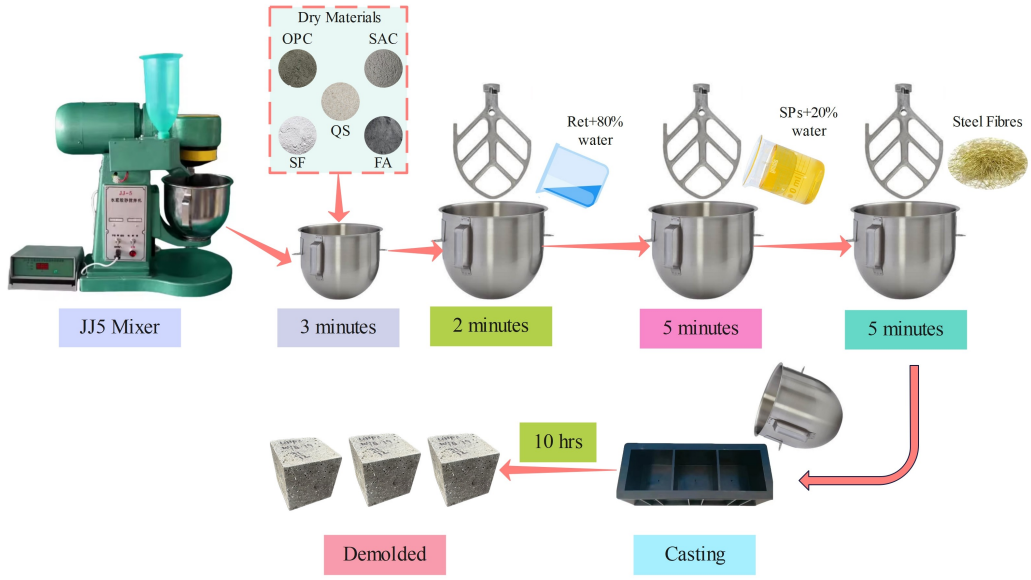


Figure 6. Step-by-step illustration of the mixing and de-molding procedure.

2.6. Curing Regime

Specimens remain in the molds for approximately 10 h and are then demolded and cured by full immersion in saturated limewater within a curing tank at 20 °C (±2 °C) according to ASTM C109 [49] until testing. The immersion condition corresponds to a relative humidity of 100%, ensuring complete moisture availability for continuous hydration.

2.7. Testing Methods

Workability was assessed immediately after mixing using the ASTM-C1437 [50] by the slump flow method. Compressive strength was determined at 7 and 28 days on three replicate cubes from each mix in accordance with ASTM-C39 [51]. Hardened density, calculated from specimen mass and dimensions recorded prior to compressive testing per standard practice, ranged from 2459 kg/m^3 to 2510 kg/m^3 across all 32 mixtures, confirming efficient particle packing and minimal entrapped air consistent with the optimized mix design. Dimensional stability was qualitatively assessed by periodic measurement of specimen length using vernier calipers at 1, 3, 7, 14, and 28 days.

Comprehensive microstructural characterization was conducted using SEM, XRD and FTIR to elucidate the mechanisms governing strength development in mixtures incorporating liquid (LSP) and powder (PSP) superplasticizers. To correlate microstructural evolution

with mechanical performance, specimens exhibiting extreme compressive strength values (both high and low) were selectively analyzed. Quantitative SEM image analysis was performed using Python-based image processing libraries (OpenCV, scikit-image) executed in Google Colab. Micrographs were converted to 8-bit grayscale, smoothed with a Gaussian filter ($\sigma = 1.5$) to reduce beam noise, and enhanced via adaptive histogram equalization. Pore phases were segmented using Otsu's automated thresholding method to calculate the 2D area porosity. The workflow was validated against ImageJ 1.54s on a 20% random subset, yielding $< 3\%$ deviation in area fraction. Results represent relative 2D area fractions for comparative mixture evaluation.

2.8. Statistical Analysis

Statistical rigor is ensured through the use of a paired *t*-test, comparing the compressive strength of each LSP and PSP mix pair, and a two-way ANOVA, examining the main and interaction effects of SP form and w/b ratio on compressive strength. A significance level of $\alpha = 0.05$ is adopted. Coefficient of variation (CV = SD/mean × 100%) was calculated for triplicate specimens at each age to quantify test repeatability and enable comparison with accepted variability limits for UHPC testing.

3. Results and Discussion

This research helps to draw a line between two different forms of SPs used in UHPC to evaluate the use and effect of these SPs on the workability and compressive strength of UHPC. The microstructure and the chemical composition of the samples help to depict a clear image of the effect of the SPs physical form. As SAC is a new type of cementitious material introduced in UHPC, this study also investigates the effect of dosage of SAC on workability and compressive strength.

3.1. Workability

The workability method used in this study is standardized by ASTM-C1437 [50] as shown in Figure 7. In this research, both LSPs and PSPs significantly influence the workability of UHPC. The incorporation of SPs enhances the flowability and reduces the water demand, which is critical for achieving the desired working time and dense microstructure of UHPC.

Table 6 and Figure 8 clearly illustrate the substantial effect of the physical form of superplasticizer on the workability of UHPC mixtures. For all binder combinations and water-to-binder (w/b) ratios tested, the use of liquid superplasticizers (LSPs) results in significantly higher flowability compared to powder superplasticizers (PSPs). For example, Mix 59 with LSP achieves a spread diameter of 255 mm, whereas the equivalent Mix 60 with PSP only reaches 175 mm. This trend is consistently observed across all paired mixes, with the LSP mixes exhibiting an average of 40–50% higher spread values. As shown in Figure 8, the increase in spread is not only attributed to the chemical composition but also to the rapid solubility and uniform dispersion of the liquid superplasticizer within the mix. The improved dispersion enhances particle lubrication, reduces internal friction, and promotes a more workable mix. The markedly lower slump flow observed with the powder PCE is linked to its delayed dissolution and incomplete particle adsorption during early mixing, particularly under low w/b ratios. Additionally, the slight increase in spread observed in mixes with higher OPC content (e.g., Mix 67 vs. Mix 59) is due to the lower water demand of OPC compared to SAC. Thus, by decreasing the SAC while maintaining a constant binder content, the flowability of the mixture increases gradually, further amplifying the benefit of LSPs. This result highlights that for UHPC applications where high workability

is essential, LSPs provide a significant advantage in achieving flow without increasing the w/b ratio, which is critical for maintaining the dense microstructure and high strength.



(a) (b)

Figure 7. Comparison of slump flow values for LSPs (**a**) and PSPs (**b**).

Table 6. Workability of UHPC mixes with different SP types and w/b ratios.

Mix ID	w/b Ratio	SP Type	SP Dosage (%)	Spread (mm)
59	0.21	LSPs	1.0	255
60	0.21	PSPs	1.0	175
61	0.20	LSPs	1.0	250
62	0.20	PSPs	1.0	170
63	0.19	LSPs	1.0	242
64	0.19	PSPs	1.0	160
65	0.18	LSPs	1.5	239
66	0.18	PSPs	1.5	154
67	0.21	LSPs	1.0	267
68	0.21	PSPs	1.0	179
69	0.20	LSPs	1.0	267
70	0.20	PSPs	1.0	175
71	0.19	LSPs	1.0	250
72	0.19	PSPs	1.0	159

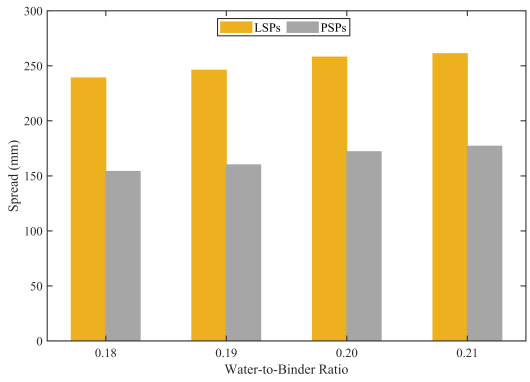


Figure 8. Comparison of slump flow values for LSPs and PSPs.

3.2. Compressive Strength

The compressive strength results of 7 and 28 days for all 32 specimens shown in Figure 9, are summarized in Table A2 and visualized in Figures 10 and 11. Data dispersion is quantified using standard deviation (SD) and coefficient of variation (CV). Across all mixtures, CV values range from 3.2% to 7.8% (mean 5.1% at 28 days), falling within accepted limits for fiber-reinforced UHPC (ASTM C109 [49]; fib Bulletin 38). LSP mixes

consistently exhibit lower CV than PSP counterparts (4.8% vs. 5.4%, $p = 0.042$), supporting improved mixing homogeneity. Figure 10 shows the direct paired comparison of compressive strengths between LSP and PSP mixes for each mix design. It is evident that in all matched pairs, the mixes incorporating LSPs consistently outperform those with PSPs. Mix Pair 59 and 60 demonstrates a 3.7 MPa strength gain (73.7 MPa vs. 71.1 MPa) for 7 days and 3.3 MPa difference for 28 days in favor of LSPs. More significantly, at lower w/b ratios, this strength difference is widened. Mix Pair 65 and 66 shows compressive strengths of 75.2 MPa for LSPs compared to 63.1 MPa for PSPs at 7 days, and this difference even increases at 28 days of curing to 101.3 MPa for LSPs and 85.6 MPa for PSPs for a lower w/b ratio of 0.18. The maximum strength recorded is 95.9 MPa at 7 days and 112.1 MPa at 28 days which is achieved with an LSPs mix (Mix 71). Conversely, Mixes 73 and 74 exhibit the lowest compressive strength values (79.3 MPa and 67.5 MPa at 28 days, respectively). This reduction is attributed to these mixes incorporating the highest water-to-binder ratio (0.21) combined with a lower silica fume content (124 g) compared to other formulations (e.g., Mix 59 with 185 g silica fume). Figure 11 presents the average compressive strength across all specimens for each SP type. The results confirm that the LSP mixes achieve an average 7-day compressive strength of 80.1 MPa, while the PSP mixes average 72.8 MPa, an approximate 10% improvement. The enhanced strength performance is directly linked to the faster dispersion and immediate availability of LSPs to adsorb onto cement particles, promoting denser hydration products at early ages.

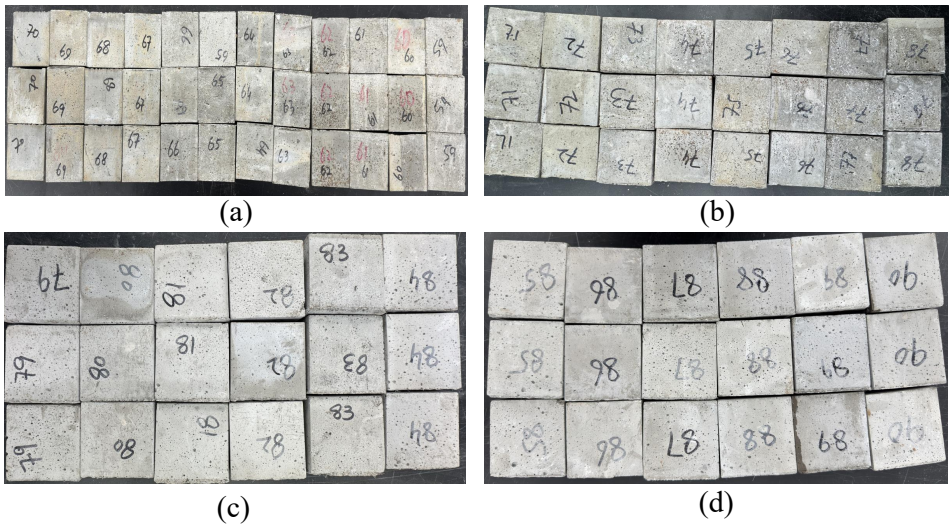
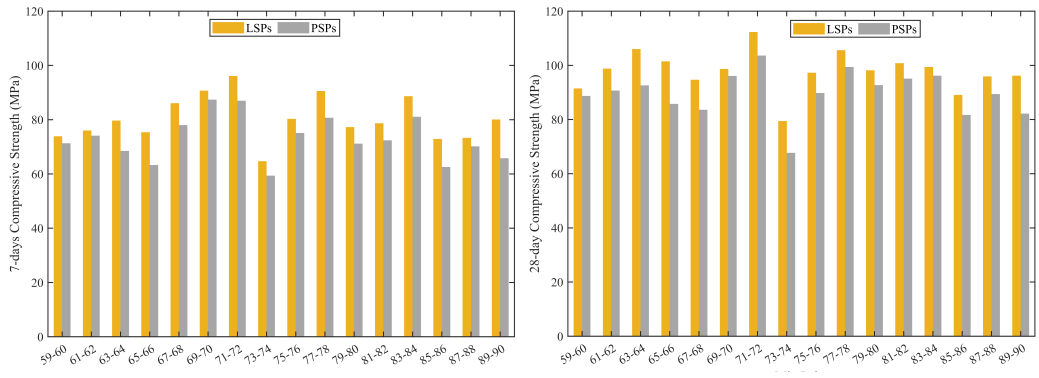


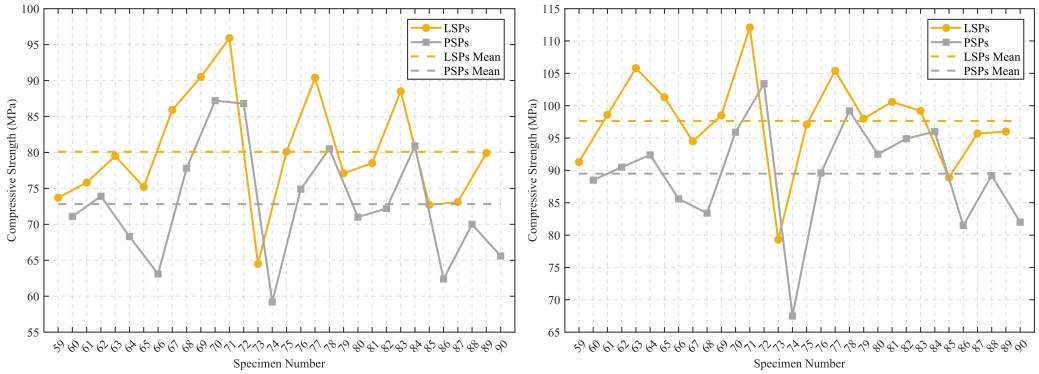
Figure 9. Samples for testing (**a**) 59–70, (**b**) 71–78, (**c**) 79–84, and (**d**) 85–90.



(**a**) (**b**)

Figure 10. Paired comparison of compressive strength between LSP and PSP mixes at (**a**) 7 days and (**b**) 28 days across varying w/b ratios.

The maximum 28-day compressive strength achieved in this study is 112.1 MPa (Mix 71);this strength range (90–112 MPa) is consistent with peer-reviewed reports on ambient-cured UHPC systems where thermal treatment is omitted. This value is below the >150 MPa threshold often associated with heat-cured UHPC; it represents a high-performance benchmark for ambient-cured SAC-based systems. The focus of this study is to isolate the influence of superplasticizer form under practical curing conditions (20 °C water curing) rather than to maximize strength through steam curing. Recent studies on ambient-cured UHPC indicate that strengths exceeding 100 MPa are achievable and structurally significant when optimized for particle packing and fiber reinforcement. Therefore, the observed strength gains attributed to the liquid superplasticizer are critical for practical applications where thermal curing is economically or logistically unfeasible. The average strength of all the specimens is compared and denoted graphically in Figure 11, which clearly states that for every mix design, the values of the compressive strength of LSPs are higher than for the PSPs.



(**a**) (**b**)

Figure 11. Comparison of compressive strength values for matched pairs of UHPC specimens at varying water-to-binder (w/b) ratios, tested at (**a**) 7 days and (**b**) 28 days.

Influence of SAC/OPC Ratio

The results in Figure 12 show a clear correlation between the SAC/OPC ratio and UHPC compressive strength. At low ratios (<1.0), OPC dominates hydration, leading to slower early strength. Increasing SAC accelerates ettringite and C-A-S-H formation, refining the pore structure and enhancing strength, particularly with liquid PCE due to superior particle dispersion. Beyond SAC/OPC ratios of 3.0–4.0, strength plateaus as aluminate-rich hydration stabilizes. Liquid PCE consistently outperforms powder, achieving the highest 28-day strength of 112 MPa at a ratio of 4.0.

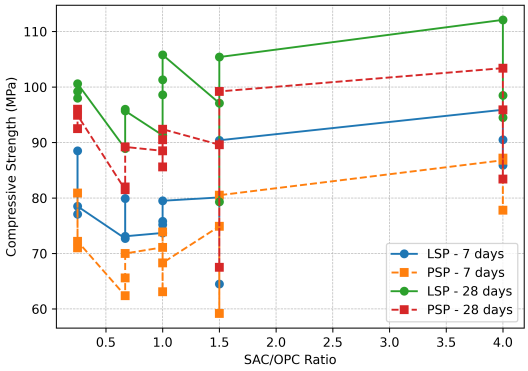


Figure 12. Variation of 7- and 28-day compressive strength of SAC-UHPC with SAC/OPC ratio for LSPs and PSPs.

3.3. Failure Mode

To evaluate matrix homogeneity and fiber–matrix interaction, post-compression failure modes are classified according to the ASTM C39 [52] guidelines and established UHPC fracture mechanics frameworks. High-resolution images of all tested specimens as shown in Figure 13 are analyzed to measure primary crack inclination angles relative to the loading axis, with failure modes categorized as: axial splitting (0°–15°), diagonal shear (30°–60°), or spalling (>60°/multi-branching). Quantitative analysis reveals that LSP specimens predominantly fail via axial splitting (74.2% frequency), indicating homogeneous stress distribution and improved matrix continuity (Figures A1 and 14). In contrast, PSP specimens exhibit significantly higher rates of diagonal shear cracking (52.1%) and surface spalling, reflecting localized microstructural discontinuities and incomplete particle dispersion. Crack angle measurements show a mean inclination of $8.4° \pm 3.1°$ for LSP specimens versus $38.7° \pm 9.4°$ for PSP specimens ($p < 0.001$, two-sample t-test). These failure patterns independently corroborate the SEM and XRD findings; the immediate dispersion capability of LSPs promotes uniform hydration and dense matrix formation, whereas the dissolution lag of PSPs leads to localized weaknesses that manifest as shear-dominated failure under compressive loading. This mechanical validation reinforces the study's conclusion that the superplasticizer physical form directly governs structural integrity in ambient-cured SAC-UHPC.



Figure 13. Representative post-compression failure modes. Mix 71 (LSP) exhibits axial splitting; Mix 72 (PSP) shows diagonal shear cracking; Mix 74 (PSP) demonstrates spalling. High-contrast imaging highlights crack patterns and fracture surfaces.

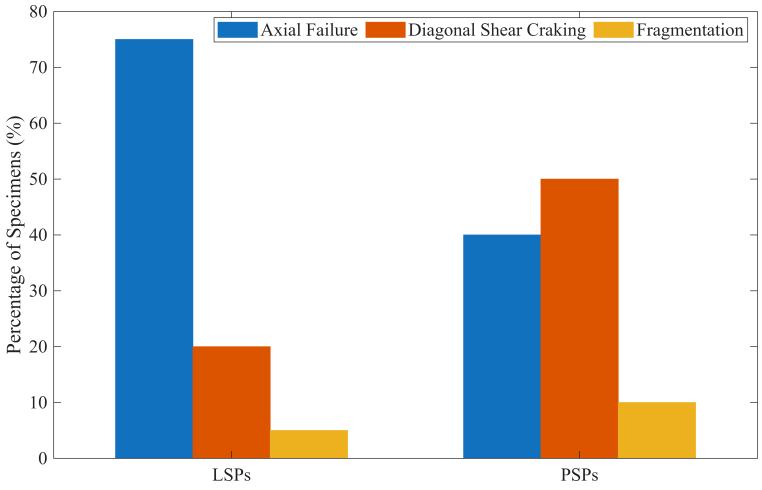


Figure 14. Frequency of axial versus shear failure modes in LSP and PSP specimens.

3.4. Statistical Analysis of Strength Differences

Statistical analyses were conducted to evaluate the effects of superplasticizer physical form on the UHPC compressive strength. All analyses were performed using Python (SciPy 1.16.3/StatsModels 0.14.6) with significance threshold $\alpha = 0.05$.

3.4.1. Paired *t*-Test Analysis

Paired *t*-tests compared the 16 matched mixture pairs (LSP vs. PSP at identical binder composition and w/b ratio) using Equation (1):

$$t = \frac{\bar{d}}{s_d/\sqrt{n}} \tag{1}$$

where $\bar{d}$ is the mean difference in compressive strength between LSP and PSP specimens, s_d is the standard deviation of paired differences, and $n = 16$ is the number of pairs.

Results demonstrate statistically significant advantages for LSP mixtures at both 7 days ($t(15) = 7.91$, $p < 0.001$) and 28 days ($t(15) = 8.52$, $p < 0.001$), with mean strength improvements of 7.28 MPa and 8.39 MPa, respectively (Table 7). These results confirm that the liquid superplasticizer form consistently enhances compressive strength under identical mix conditions.

Table 7. Paired *t*-test results comparing compressive strength of UHPC specimens with powder (PSP) and liquid (LSP) superplasticizers. Values represent mean difference ± standard deviation of differences.

Test Age	Mean Difference (MPa)	*t*(15)	*p*-Value
7 days	7.28 ± 3.68	7.91	<0.001
28 days	8.39 ± 3.94	8.52	<0.001

3.4.2. Two-Way ANOVA: Main and Interaction Effects

A two-way analysis of variance (ANOVA) is employed to examine the main effects of the superplasticizer form and water-to-binder ratio, as well as their interaction, on compressive strength. The statistical model is defined by Equation (2):

$$Y_{ijk} = \mu + \alpha_i + \beta_j + (\alpha\beta)_{ij} + \epsilon_{ijk} \tag{2}$$

where Y_{ijk} represents the compressive strength observation, μ is the overall mean, α_i is the effect of the superplasticizer type (i = LSP, PSP), β_j is the effect of the water-to-binder ratio ($j = 0.18, 0.19, 0.20, 0.21$), $(\alpha\beta)_{ij}$ is the interaction effect, and $\epsilon_{ijk} \sim \mathcal{N}(0, \sigma^2)$ is the random error term. *F*-statistics are computed as $F = MS_{\text{effect}}/MS_{\text{residual}}$.

Residual diagnostics confirm that the ANOVA assumptions are satisfied, residuals exhibit approximate normality (Shapiro–Wilk test: $p = 0.18$ for 7 days, $p = 0.23$ for 28 days) and homogeneity of variance (Levene's test: $p = 0.31$ for 7 days, $p = 0.27$ for 28 days).

Analysis reveals significant main effects for both the superplasticizer form and water-to-binder ratio at both curing ages (Table 8). Critically, the SP × w/b interaction term is not statistically significant ($p = 0.763$ at 7 days; $p = 0.809$ at 28 days), indicating that the performance advantage of liquid superplasticizers is consistent across the tested water-to-binder ratio range (0.18–0.21).

Effect size interpretation via partial η^2 further clarifies the practical importance. The superplasticizer form exhibits a large effect ($\eta^2 = 0.24$–0.34), explaining 24–34% of the variance in compressive strength. The water-to-binder ratio likewise demonstrates a large effect ($\eta^2 = 0.32$–0.44), consistent with the established UHPC behavior. The SP × w/b

interaction shows a negligible effect ($\eta^2 = 0.04$–0.05), confirming that the directional benefit of LSP does not systematically vary with the w/b ratio within the ultra-low range studied.

These statistical findings support the conclusion that liquid superplasticizers provide robust, w/b-independent improvements in compressive strength for SAC-based UHPC under ambient curing conditions. The non-significant interaction aligns with the proposed kinetic mechanism: because liquid PCE achieves immediate dispersion regardless of the available mixing water, its advantage persists across ultra-low w/b ratios, where powder PCE dissolution kinetics become rate limiting.

Table 8. Two-way ANOVA summary showing the effects of the superplasticizer type (SP), water-to-binder ratio (w/b), and their interaction on UHPC compressive strength. Partial η^2 indicates the effect size (small: <0.06, medium: 0.06–0.14, large: >0.14).

Source	SS	df	MS	*F*	*p*-Value	Partial η^2
(a) 7-day Compressive Strength						
Superplasticizer (SP)	423.40	1	423.40	7.54	0.011	0.239 (Large)
Water-to-Binder Ratio (w/b)	629.67	3	209.89	3.74	0.025	0.318 (Large)
SP × w/b Interaction	65.42	3	21.81	0.39	0.763	0.046 (Small)
Residual	1348.04	24	56.17	—	—	—
Total	2466.54	31	—			
(b) 28-day Compressive Strength						
Superplasticizer (SP)	529.75	1	529.75	12.25	0.002	0.338 (Large)
Water-to-Binder Ratio (w/b)	827.80	3	275.93	6.38	0.003	0.444 (Large)
SP × w/b Interaction	41.93	3	13.98	0.32	0.809	0.039 (Small)
Residual	1037.94	24	43.25	—	—	—
Total	2437.42	31	—			

The point plot of compressive strength for UHPC specimens containing powder (PSP) and liquid superplasticizers (LSP) with varying binder compositions and water-to-binder ratios is shown in Figure 15. LSP specimens show higher median strength and lower variability than PSP specimens. Paired *t*-tests and two-way ANOVA are used for statistical analysis and are tabulated in Table 7 and Table 8, respectively.

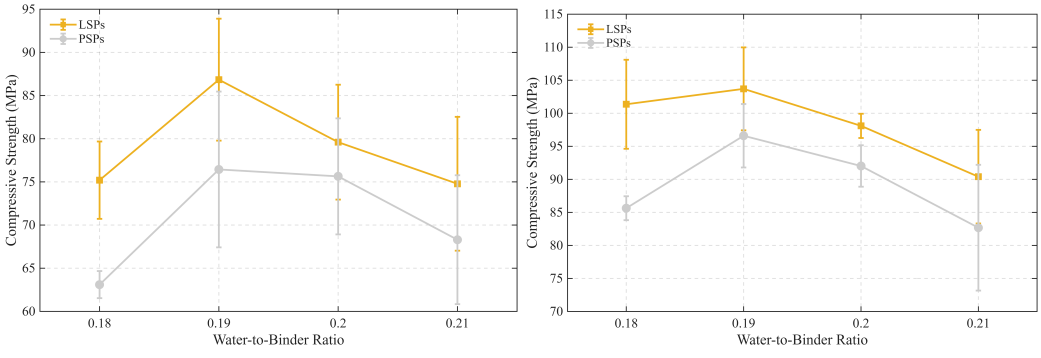


Figure 15. Variation of compressive strength with w/b ratio for UHPC incorporating PSPs and LSPs at (**a**) 7 days and (**b**) 28 days.

3.5. Scanning Electron Microscopy (SEM) Analysis

The microstructural evaluation of SAC-based UHPC is carried out using SEM at a magnification of 10,000×. Quantitative image analysis is performed using threshold-based segmentation with adaptive contrast enhancement and morphological filtering to determine porosity percentage, pore size distribution, and crack density from the SEM

micrographs. Figure 16a,c correspond to specimens incorporating LSPs (Mixes 71 and 85), whereas Figure 16b,d represent specimens prepared with PSPs (Mixes 72 and 86).

Quantitative image analysis (Table 9) reveals that LSP specimens exhibit lower total porosity compared to PSP specimens. Mix 71 (LSP) shows 9.90% porosity versus 14.41% for Mix 72 (PSP), representing a 31.3% reduction. Similarly, Mix 85 (LSP) exhibits 11.44% porosity compared to 13.30% for Mix 86 (PSP), a 14.0% reduction. The average porosity reduction of 23.0% in LSP mixes correlates strongly with the observed 10.3% increase in compressive strength, supporting the hypothesis that improved particle dispersion promotes denser matrix formation in SAC-based UHPC. These porosity values represent 2D area fractions and should be interpreted as relative comparative indicators rather than absolute volumetric measurements. Accordingly, descriptions of a "dense, well-packed matrix" reflect the qualitative and semi-quantitative microstructural trends observed via SEM, rather than direct density or MIP validation.

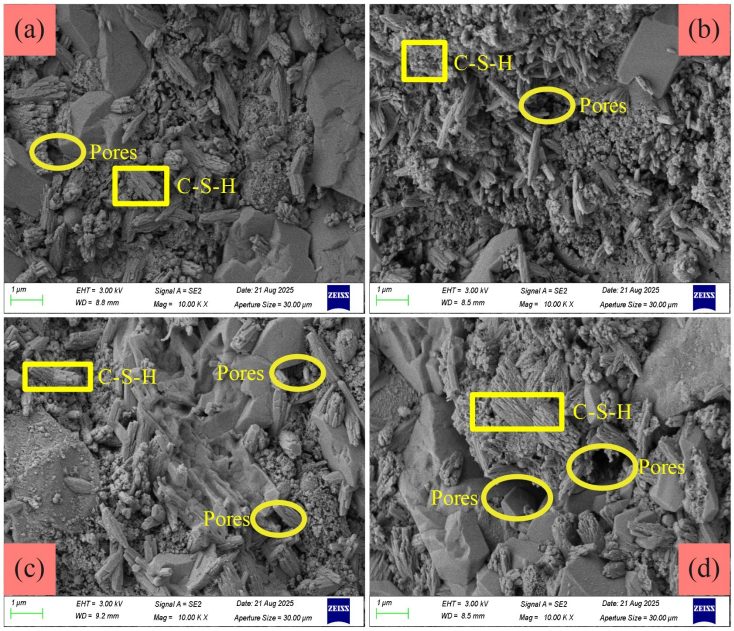


Figure 16. SEM analysis after 28 days (**a**) 71, (**b**) 72, (**c**) 85, and (**d**) 86.

The pore size distribution analysis demonstrates that all mixes contain predominantly fine pores (<1 μm), accounting for 99.5–100% of the detected pores. Average pore diameters range from 0.150 to 0.180 μm with no systematic difference between SP forms, indicating that the physical form of the superplasticizer primarily influences pore quantity rather than pore size refinement under ultra-low w/b conditions.

Crack density analysis shows low and variable values across specimens (0.0–0.0132 μm^{-2}), with no consistent pattern between SP forms. This suggests that discrete microcracking is not the dominant factor influencing strength in these low w/b systems; rather, the overall porosity and pore connectivity govern mechanical performance.

The micrographs of LSP mixes exhibit a dense and well-packed matrix characterized by the extensive formation of needle-shaped ettringite and finely intergrown calcium silicate hydrate (C-S-H) phases. Plate-like crystals are embedded in a continuous hydration network with minimal visible capillary pores. In contrast, specimens containing powder superplasticizer show a comparatively porous microstructure with discontinuous hydration products and less uniform C-S-H distribution. The ettringite needles are shorter and less densely arranged, and unreacted particles remain visible within the matrix.

The pore size distribution further reveals that while all mixes contain predominantly fine pores (<1 μm), PSP Mix 72 exhibits the highest proportion of larger pores (≥1 μm) at

0.5%, compared to 0.0% for LSP mixes. This shift toward coarser porosity in PSP specimens indicates less efficient particle packing and incomplete hydration.

These quantitative microstructural observations demonstrate that the physical form of the superplasticizer significantly influences particle dispersion, hydration kinetics, pore structure refinement, and crack formation, all of which directly affect the mechanical performance of SAC-based UHPC. The lower porosity observed in LSP mixes provides a mechanistic explanation for their superior compressive strength and axial failure modes, confirming that the superplasticizer physical state is a critical parameter governing microstructural development in SAC-based UHPC under ultra-low water conditions.

Table 9. Quantitative SEM image analysis results showing porosity, pore size distribution, and crack characteristics of UHPC specimens with liquid (LSP) and powder (PSP) superplasticizers.

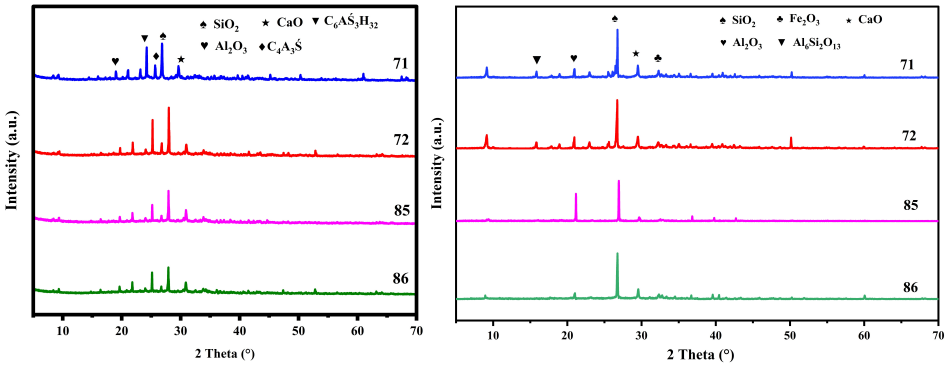
Specimen ID	SP Type	Porosity (%)	Pore Count	Avg Pore Size (μm)	Crack Density (1/μm^2)	Small Pores <1 μm (%)	Large Pores ≥1 μm (%)
71	LSP	9.90	256	0.154	0.0132	100.0	0.0
72	PSP	14.41	344	0.150	0.0000	100.0	0.0
85	LSP	11.44	262	0.160	0.0000	100.0	0.0
86	PSP	13.30	194	0.180	0.0090	99.5	0.5
Avg LSP	–	10.67	259	0.157	0.0066	100.0	0.0
Avg PSP	–	13.86	269	0.165	0.0045	99.8	0.3
Reduction	–	23.0%	–	–4.8%	–	+0.2%	–100%

3.6. X-Ray Diffraction Analysis (XRD)

To isolate the effects of the SP form and w/b ratio on phase evolution, XRD analysis is conducted on a representative subset of four mixtures: LSP/PSP pairs at w/b ratios of 0.19 (Mixes 71 and 72) and 0.21 (Mixes 85 and 86). The effects of different superplasticizers (liquid PCE vs. powder PCE) on the hydration products are compared. The XRD patterns (Figure 17) show that in the 20°–30° range, the characteristic peak full width at half maximum (FWHM) of sample 71 (liquid PCE, w/b = 0.19) and sample 85 (liquid PCE, w/b = 0.21) are significantly larger than those of sample 72 (powder PCE, w/b = 0.19) and sample 86 (powder PCE, w/b = 0.21). This indicates that the liquid superplasticizer effectively promotes the formation of an amorphous C-S-H gel. This is related to the molecular structural characteristics of liquid PCE: its polycarboxylate backbone, through electrostatic repulsion and steric hindrance effects, rapidly adsorbs onto the surface of cement particles at the initial mixing stage, effectively dispersing agglomerates of cementitious materials and fully exposing the reactive surfaces of fly ash and silica fume, thereby accelerating the pozzolanic reaction process. In sample 71, the characteristic peak intensities of quartz (SiO_2) and mullite ($Al_6Si_2O_{13}$) are lower than in sample 72, indicating that liquid PCE, by optimizing the particle packing density, facilitates the dissolution of aluminosilicate mineral phases, thus generating more low-crystallinity C-S-H gel.

In the powder PCE group, the higher retention of the quartz peak in the XRD patterns suggests that the dissolution kinetics of powder PCE are slower, and during the initial mixing stage it is not fully released, causing part of the silica fume particles to remain encapsulated by unhydrated cement, thereby delaying their participation in secondary reactions. For low water-to-binder ratio systems, liquid PCE plays a more critical role in improving workability by lowering the yield stress of the paste, allowing nano-scale silica fume to be more evenly distributed within the cement matrix, thus enhancing early hydration efficiency. Comparing the influence of the water-to-binder ratio further, in the liquid PCE group the mullite peak intensity retention in sample 85 (w/b = 0.21) is higher than in sample 71 (w/b = 0.19), indicating that a higher water-to-binder ratio weakens the dispersion advantage of liquid PCE: the excess free water dilutes the adsorption concen-

tration of PCE molecules on particle surfaces, leading to reduced dispersion efficiency. In the powder PCE group, the quartz peak intensity retention in sample 86 (w/b = 0.21) is only slightly lower than in sample 72 (w/b = 0.19), suggesting that powder PCE is less sensitive to water-to-binder ratio, with its effectiveness relying more on the sustained dispersion effect provided by continuous dissolution over time. This difference is associated with the physical form of the superplasticizer: liquid PCE is pre-dissolved in mixing water and can act immediately, whereas powdered PCE must undergo water absorption and swelling as well as chain extension, making its dispersion efficiency time dependent and therefore limited in low water-to-binder, high-viscosity systems. The XRD results demonstrates that the liquid PCE, by promoting the abundant early formation of C-S-H gel, optimizes the structure of the interfacial transition zone, thereby improving the matrix density and mechanical performance. While this targeted selection effectively captures comparative phase evolution trends, the findings reflect specific binder ratios and should be interpreted as indicative of relative hydration pathways rather than fully generalizable across all 32 mix designs.



(**a**) (**b**)

Figure 17. X-ray diffraction analysis: (**a**) 7 days and (**b**) 28 days.

3.7. Fourier Transform Infrared Analysis (FTIR)

FTIR spectra (Figure 18) further reveal the regulatory mechanism of different types of PCE superplasticizers on the chemical bond structure of hydration products. In the liquid PCE group, the main vibration peak of Si-O-Si/Si-O-Al (1110 cm^{-1}) shows an increased full width at half maximum compared with that of the powder PCE group and shifted toward higher wavenumbers, indicating that liquid PCE promoted the incorporation of Al^{3+} into the C-S-H gel structure, leading to the formation of more C-A-S-H phases. This substitution enhances the crosslinking degree of the gel network through the connection of AlO_4 tetrahedra with SiO_4 chains, thereby improving the compressive strength. In addition, the O–H stretching vibration peak (3451 cm^{-1}) in the liquid PCE group exhibits lower intensity than that in the powder group, reflecting its more efficient promotion of Ca-source consumption. The rapid dispersion effect of liquid PCE allows more complete hydration of the cement particles, where the generated Ca^{2+} reacts with reactive $SiO_2$and Al_2O_3 to form C-S-H, reducing the residual amount of free $Ca(OH)_2$.

For the powder PCE group, the characteristic peak intensity of CO_3^{2-} at 1438 cm^{-1} is higher than that in the liquid group, which is associated with the delayed dispersion of powder PCE; insufficient early dispersion results in higher porosity inside the paste, accelerating CO_2 diffusion into the interior and promoting the carbonation of more $Ca(OH)_2$ into $CaCO_3$. In sample 72 (powder PCE, w/b = 0.19), the O-H bending vibration peak at 1647 cm^{-1} is stronger than that in sample 71 (liquid PCE, w/b = 0.19), indicating a higher content of absorbed water inside, caused by uneven dispersion and incomplete local hydration, which forms micro pore defects. These structural features can act as stress

concentration sites, reducing the actual load-bearing capacity of the material. In the broad band region of 3000–3600 cm^{-1}, the peak shape of the liquid PCE group shows a trend toward enhanced symmetry, which is related to the strengthening of the hydrogen bonding network of structural water in the C-S-H gel. Infrared analysis reveals that the physical form of the superplasticizer (liquid/powder) influences the macroscopic mechanical performance of the material by regulating hydration kinetics and product microstructure.

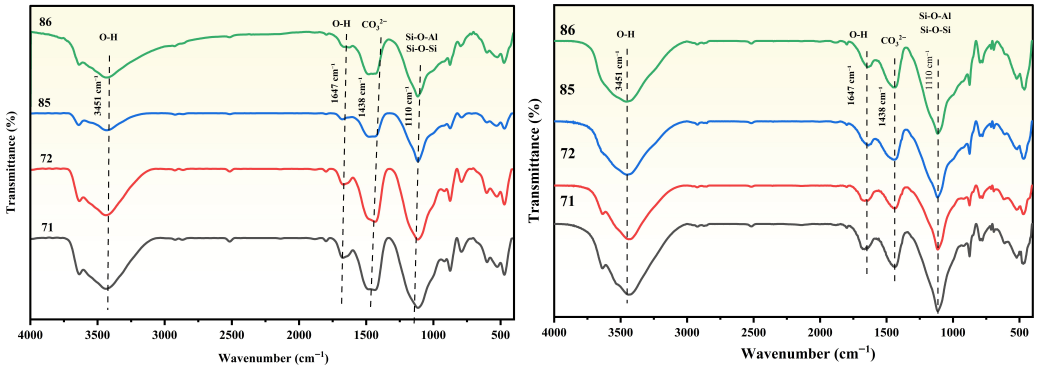


Figure 18. Fourier transform infrared analysis: (**a**) 7 days and (**b**) 28 days.

3.8. Hydration Effects and Strength Development

The observed performance differences between LSP and PSP mixtures are consistent with a kinetic mismatch hypothesis, wherein the rapid hydration kinetics of SAC may compete with the dissolution and dispersion kinetics of powder superplasticizers. While this study does not employ time-resolved techniques (e.g., isothermal calorimetry or in situ rheology) to directly quantify adsorption or dissolution rates, the macro- and microstructural findings align with established PCE dispersion mechanisms. Specifically, the immediate availability of pre-dissolved LSPs likely facilitates faster initial particle deflocculation and earlier steric stabilization, whereas PSPs may experience a time-dependent dissolution lag that coincides with accelerated SAC ettringite formation. The 28-day XRD and FTIR results reflect end-state microstructural differences that support this proposed kinetic pathway, though they do not capture real-time hydration dynamics. Consequently, the kinetic mismatch framework is presented here as a working hypothesis to interpret the observed workability, strength, and porosity trends. Direct validation using time-resolved measurements is recommended for future investigations to confirm the exact adsorption–dissolution–hydration interplay in ultra-low w/b SAC systems.

4. Conclusions

This research presents a detailed investigation to quantify the influence of superplasticizer form on the fresh and hardened performance of SAC based UHPC at water–binder ratios between 0.18 and 0.21. All mix parameters other than the physical state of the PCE superplasticizer were kept constant to isolate this variable. The findings are categorized below into fundamental materials science outcomes and practical engineering implications.

4.1. Scientific Findings

1. Rheological Enhancement: Liquid superplasticizers (LSP) consistently improved slump flow spread by 40–50% relative to powder equivalents (PSP). This gain was achieved without increasing water content, indicating superior particle lubrication and reduced internal friction due to immediate polymer availability.
2. Mechanical Performance: Mixtures incorporating LSP demonstrated a statistically significant increase in compressive strength, averaging 7–9 MPa higher at 7 days

compared to PSP mixes. The maximum 28-day strength recorded was 112.1 MPa (Mix 71), confirming that ambient-cured SAC-UHPC can achieve high-performance benchmarks without thermal treatment.

3. Statistical Validation: Paired *t*-tests and two-way ANOVA verified that the superplasticizer form is a dominant variable affecting strength ($p < 0.001$). The interaction effects indicate that the advantage of liquid forms remains robust across varying water-to-binder ratios.
4. Microstructural Refinement: Quantitative SEM analysis indicated a 23.0% reduction in total porosity for LSP specimens (10.67%) compared to PSP (13.86%). This densification correlates directly with strength gains and is characterized by a predominance of fine pores (<1 μm).
5. Failure Mechanics: Fracture patterns diverged significantly between forms. LSP specimens failed primarily through axial fracture (75% frequency), suggesting homogeneous stress distribution. In contrast, PSP specimens exhibited diagonal shear cracking and spalling (50% frequency), indicative of microstructural discontinuities.
6. Kinetic Mechanism: The study identified a kinetic mismatch specific to rapid-setting binders. SAC hydration rates (initial set ≈ 20 min) exceed the dissolution and chain-extension kinetics of powder superplasticizers. This lag results in incomplete dispersion and localized defects in PSP mixes, whereas pre-dissolved LSPs ensure immediate steric stabilization before matrix stiffening.

4.2. Engineering Recommendations and Economic Implications

While the demonstrated improvements in workability and compressive strength suggest potential benefits for precast and fast-track applications, direct validation of formwork stripping schedules, energy savings, quality assurance metrics, and logistical trade-offs would require dedicated early-age testing, life-cycle assessment, and field-scale trials beyond the scope of this study.

5. Future Recommendation and Limitations

Further work should examine the optimum dosage for both physical types, 1-day compressive strength, flexural strength, long-term durability and the influence of variable curing regimes to extend these conclusions to broader field conditions. The ultra-low w/b ratios (0.19–0.21) and high binder content are expected to induce significant autogenous shrinkage, which was not measured here and should be evaluated for long-term dimensional stability.

Author Contributions: A.S.: Writing—review and editing, Writing—original draft, Software, Formal analysis, Visualization, Conceptualization, Data curation. E.X.: Supervision, Resources, Funding acquisition, Conceptualization. M.A.S.: Validation, Software, Data curation and M.H.: Visualization, Writing—review. All authors have read and agreed to the published version of the manuscript.

Funding: This research received no external funding.

Institutional Review Board Statement: This research involved no human or animal subjects. All experiments were performed using construction materials in accordance with standard laboratory practices and safety protocols.

Data Availability Statement: The datasets generated and analyzed during the current study, including processed experimental data and supporting analysis materials, are available from the corresponding author upon reasonable request.

Conflicts of Interest: The authors declare that they have no known competing financial interests or personal relationships that could have appeared to influence the work reported in this paper.

Appendix A

Appendix A.1. Mix Proportions

Table A1. Mix proportions of specimens (all quantities in kg/m^3) (SAC: Sulfoaluminate Cement, OPC: Ordinary Portland Cement, SF: Silica Fume, FA: Fly Ash, w/b: water-to-binder ratio, QS: Quartz Sand, sf: Steel Fiber, SP: Superplasticizer, Ret: Retarder).

ID	SAC	OPC	SF	FA	w/b	QS	sf	SP	Ret	Water
59	380.2	380.2	152.3	101.2	0.21	1015.6	231.3	16.92	10.16	212.9
60	382.9	382.9	153.3	101.9	0.21	1022.7	232.9	10.23	10.23	214.4
61	384.4	384.4	153.9	102.1	0.20	1026.4	231.3	17.08	10.25	205.0
62	387.1	387.1	155.0	102.8	0.20	1033.6	232.9	10.32	10.32	206.4
63	388.4	388.4	155.5	103.7	0.19	1036.8	231.2	17.26	10.36	196.8
64	391.2	391.2	156.6	104.4	0.19	1044.2	232.9	10.43	10.43	198.2
65	390.3	390.3	156.0	103.7	0.18	1040.4	229.5	24.96	10.40	187.3
66	394.2	394.2	157.5	104.7	0.18	1050.5	231.7	15.76	10.51	189.1
67	652.6	162.7	101.4	101.4	0.21	1019.8	229.8	16.97	10.18	213.8
68	657.2	163.9	102.1	102.1	0.21	1026.9	231.4	10.25	10.25	215.3
69	658.9	164.3	103.0	103.0	0.20	1030.0	229.7	17.15	10.29	205.8
70	663.5	165.5	103.7	103.7	0.20	1037.3	231.3	10.36	10.36	207.3
71	666.3	166.0	103.8	103.8	0.19	1041.6	229.7	17.33	10.40	197.6
72	671.1	167.1	104.6	104.6	0.19	1049.0	231.4	10.47	10.47	199.0
73	489.9	326.3	101.9	101.9	0.21	1020.8	231.0	17.00	10.20	214.2
74	493.3	328.6	102.6	102.6	0.21	1028.0	232.6	10.27	10.27	215.7
75	495.1	329.8	102.8	102.8	0.20	1032.2	231.1	17.17	10.31	206.1
76	498.6	332.1	103.5	103.5	0.20	1039.5	232.7	10.38	10.38	207.6
77	500.7	333.8	103.6	103.6	0.19	1043.3	231.0	17.36	10.42	197.9
78	504.3	336.2	104.3	104.3	0.19	1050.8	232.7	10.49	10.49	199.3
79	163.6	655.3	102.2	102.2	0.21	1024.1	233.4	17.05	10.23	214.9
80	164.8	659.9	102.9	102.9	0.21	1031.3	235.0	10.30	10.30	216.4
81	165.4	662.4	103.1	103.1	0.20	1035.6	233.5	17.23	10.34	206.8
82	166.6	667.1	103.8	103.8	0.20	1042.9	235.2	10.41	10.41	208.2
83	167.1	670.1	103.9	103.9	0.19	1046.7	233.6	17.42	10.45	198.6
84	168.3	674.9	104.7	104.7	0.19	1054.3	235.3	10.53	10.53	200.0
85	327.3	491.0	101.7	101.7	0.21	1022.5	232.3	17.03	10.22	214.6
86	329.6	494.5	102.4	102.4	0.21	1029.7	233.9	10.29	10.29	216.1
87	330.4	495.6	103.3	103.3	0.20	1033.3	232.1	17.21	10.33	206.5
88	332.7	499.1	104.0	104.0	0.20	1040.7	233.8	10.40	10.40	208.0
89	333.8	501.6	104.1	104.1	0.19	1044.5	232.2	17.39	10.44	198.3
90	336.2	505.2	104.9	104.9	0.19	1052.0	233.9	10.51	10.51	199.7

Appendix A.2. Compressive Strength Results

Table A2. Compressive strength test results of UHPC specimens at 7 and 28 days (three specimens per mix, values in MPa). SD = sample standard deviation; CV = coefficient of variation.

Specimen IDs	7 Days Compressive Strength (MPa)					28 Days Compressive Strength (MPa)				
	S1	S2	S3	Avg.	±SD (CV%)	S1	S2	S3	Avg.	SD (CV%)
59	73.6	71.9	75.7	73.7	1.90 (2.58)	85.6	94.7	93.7	91.3	4.99 (5.46)
60	72.5	70.8	70.0	71.1	1.28 (1.80)	82.4	93.9	89.5	88.5	5.80 (6.55)
61	75.7	76.4	75.4	75.8	0.51 (0.68)	102.3	100.6	93.0	98.6	4.95 (5.02)
62	76.2	75.2	70.2	73.9	3.21 (4.35)	92.3	86.4	92.5	90.5	3.47 (3.83)
63	79.8	79.4	79.4	79.5	0.23 (0.29)	109.2	103.4	105.0	105.8	3.00 (2.83)
64	72.8	64.5	67.6	68.3	4.19 (6.14)	86.9	95.3	95.0	92.4	4.77 (5.16)
65	71.9	73.4	80.3	75.2	4.48 (5.96)	107.4	102.6	94.1	101.3	6.74 (6.64)
66	62.8	64.8	61.7	63.1	1.57 (2.49)	87.3	85.9	83.7	85.6	1.81 (2.12)
67	86.3	88.3	83.2	85.9	2.57 (2.99)	89.5	90.3	103.7	94.5	7.98 (8.44)
68	79.9	76.5	77.0	77.8	1.84 (2.36)	84.2	83.5	82.6	83.4	0.80 (0.96)
69	88.7	89.4	93.4	90.5	2.54 (2.80)	103.4	92.5	99.7	98.5	5.54 (5.63)
70	86.0	92.9	82.8	87.2	5.16 (5.92)	87.8	94.6	105.3	95.9	8.82 (9.20)
71	96.6	94.9	96.2	95.9	0.89 (0.93)	109.5	117.8	109.0	112.1	4.94 (4.41)
72	82.6	92.3	85.4	86.8	4.99 (5.75)	107.5	97.8	104.9	103.4	5.02 (4.86)
73	66.7	70.5	56.3	64.5	7.35 (11.40)	82.1	80.6	75.2	79.3	3.63 (4.58)
74	58.8	58.4	60.4	59.2	1.06 (1.79)	62.9	70.2	69.4	67.5	4.00 (5.93)
75	80.0	76.3	84.0	80.1	3.85 (4.81)	101.3	97.0	93.0	97.1	4.15 (4.27)
76	83.4	74.0	67.3	74.9	8.09 (10.80)	86.9	101.2	80.7	89.6	10.51 (11.73)

Table A2. *Cont.*

Specimen IDs	7 Days Compressive Strength (MPa)					28 Days Compressive Strength (MPa)				
	S1	S2	S3	Avg.	±SD (CV%)	S1	S2	S3	Avg.	SD (CV%)
77	91.9	91.9	87.5	90.4	2.54 (2.81)	104.6	104.9	106.7	105.4	1.14 (1.08)
78	91.2	77.9	72.4	80.5	9.67 (12.01)	99.4	95.6	102.6	99.2	3.50 (3.53)
79	85.3	74.8	71.3	77.1	7.29 (9.45)	98.7	98.6	96.7	98.0	1.13 (1.15)
80	73.5	65.6	74.0	71.0	4.71 (6.63)	87.6	92.3	97.6	92.5	5.00 (5.41)
81	73.5	82.9	79.1	78.5	4.73 (6.02)	102.5	99.5	99.8	100.6	1.65 (1.64)
82	75.3	74.0	67.4	72.2	4.24 (5.86)	89.3	103.5	91.9	94.9	7.56 (7.97)
83	94.5	80.1	91.0	88.5	7.51 (8.48)	106.7	98.3	92.6	99.2	7.09 (7.15)
84	87.0	78.3	77.3	80.9	5.34 (6.60)	89.2	99.5	99.3	96.0	5.89 (6.14)
85	81.0	74.4	62.8	72.7	9.21 (12.67)	86.2	88.4	92.1	88.9	2.98 (3.35)
86	68.1	59.7	59.3	62.4	4.97 (7.97)	81.2	79.6	83.7	81.5	2.07 (2.54)
87	69.8	76.2	73.4	73.1	3.21 (4.39)	102.3	95.8	89.0	95.7	6.65 (6.95)
88	69.1	69.0	72.0	70.0	1.70 (2.43)	92.1	85.3	90.2	89.2	3.51 (3.93)
89	85.1	72.7	81.9	79.9	6.44 (8.06)	86.4	99.0	102.6	96.0	8.51 (8.86)
90	66.2	65.8	64.9	65.6	0.67 (1.01)	82.6	81.1	81.6	81.8	0.76 (0.93)

Appendix A.3. Samples After Crushing

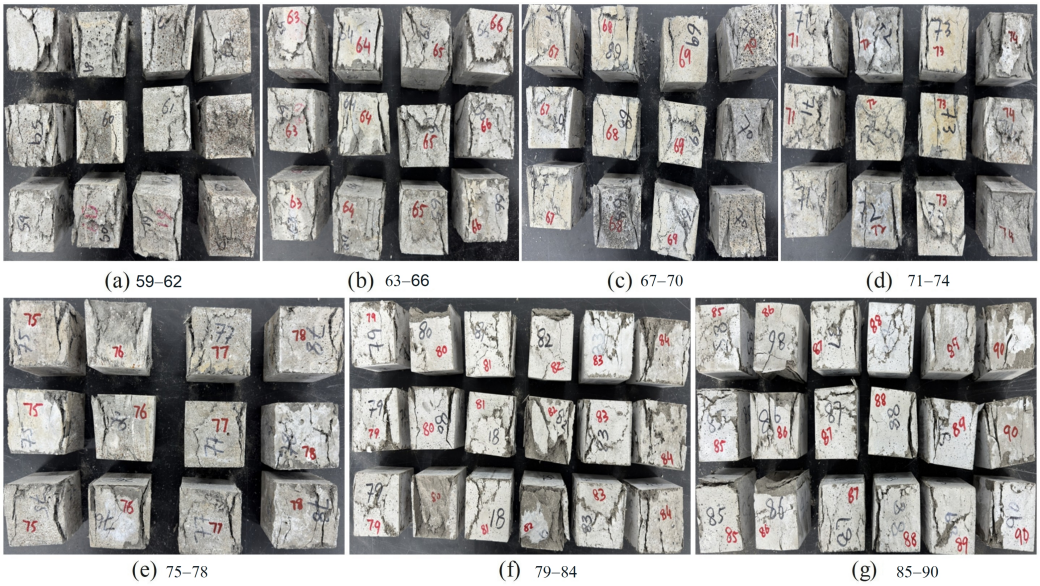


Figure A1. Samples after crushing by UTM: (**a**) 59–62, (**b**) 63–66, (**c**) 67–70, (**d**) 71–74, (**e**) 75–78, (**f**) 79–84, and (**g**) 85–90.

References

1. Richard, P.; Cheyrezy, M.H. Reactive powder concretes with high ductility and 200–800 MPa compressive strength. *Spec. Publ.* **1994**, *144*, 507–518.
2. Richard, P.; Cheyrezy, M. Composition of reactive powder concretes. *Cem. Concr. Res.* **1995**, *25*, 1501–1511. [CrossRef]
3. Resplendino, J.; Toulemonde, F. *Designing and Building with UHPFRC*; John Wiley & Sons: Hoboken, NJ, USA, 2013.
4. Nodehi, M.; Nodehi, S.E. Ultra-high performance concrete (UHPC): Reactive powder concrete, slurry infiltrated fiber concrete, and superabsorbent polymer concrete. *Innov. Infrastruct. Solut.* **2022**, *7*, 39. [CrossRef]
5. Kravanja, G.; Mumtaz, A.R.; Kravanja, S. A comprehensive review of the advances, manufacturing, properties, innovations, environmental impact, and applications of Ultra-High-Performance Concrete (UHPC). *Buildings* **2024**, *14*, 382. [CrossRef]
6. Tayeh, B.A.; Bakar, B.; Askar, L.; Askar, M.K. Ultra-High-Performance Concrete (UHPC)-Applications Worldwide: A State-of-the-Art Review. *J. Eng. Res. Technol.* **2023**, *10*, 12–27.
7. More, H.B. Design and Characterization of Ultra-High-Performance Concrete Through a Two-Step Particle Packing Optimization Method. Master's Thesis, University of Massachusetts Lowell, Lowell, MA, USA, 2023.
8. Alhajiri, A.M.; Akhtar, M.N. Enhancing sustainability and economics of concrete production through silica fume: A systematic review. *Civ. Eng. J.* **2023**, *9*, 2612–2629. [CrossRef]
9. Lallas, Z.N. Facilitating Performance-Driven Design of Innovative Prefabricated Concrete Components: Moment-Curvature Modeling and Experimental Evaluation. Ph.D. Thesis, Illinois Institute of Technology, Chicago, IL, USA, 2025.

10. Bahmani, H.; Mostofinejad, D. Microstructure of ultra-high-performance concrete (UHPC)—A review study. *J. Build. Eng.* **2022**, *50*, 104118. [CrossRef]
11. Xia, D.; Liu, H.; Liang, X. Effect of curing regimes on mechanical properties and microstructure of ultra-high performance concrete with full aeolian sand. *Constr. Build. Mater.* **2025**, *472*, 140812. [CrossRef]
12. Li, Y.; Zhao, C.; Li, H.; Liu, W. Study on the toughness and microstructure of UHPC with a high steel fiber content. *Constr. Build. Mater.* **2025**, *460*, 139810. [CrossRef]
13. Benjamin, A. *Material Property Characterization of Ultra-High Performance Concrete*; US Department of Transport: Washington, DC, USA, 2006.
14. Park, J.S.; Kim, Y.J.; Cho, J.R.; Jeon, S.J. Early-age strength of ultra-high performance concrete in various curing conditions. *Materials* **2015**, *8*, 5537–5553. [CrossRef]
15. Tamataki, K.; Ito, T.; Fujino, Y.; Yoshitake, I. Development of an ultra-high-performance fibre-reinforced concrete (UHPFRC) manufacturable at ambient temperature. *Buildings* **2022**, *12*, 740. [CrossRef]
16. Wang, X.H.; Fang, Z.C.; Zheng, L. Effect of dose and types of the water reducing admixtures and superplasticizers on concrete strength and durability behaviour: A review. *J. Civ. Eng. Manag.* **2024**, *30*, 33–48. [CrossRef]
17. Han, K.; Guo, T.; Meng, F.; Guo, Y.; Shu, X.; Ran, Q. New insight into structural build-up modification by PCE superplasticizers during early C3A hydration. *Cem. Concr. Res.* **2026**, *199*, 108048. [CrossRef]
18. Flatt, R.; Schober, I. Superplasticizers and the rheology of concrete. In *Understanding the Rheology of Concrete*; Elsevier: Amsterdam, The Netherlands, 2012; pp. 144–208.
19. Lahallh, S.M.; Absl-Halabi, M.; Ali, A.M. Effect of polymerization conditions of sulfonated-melamine formaldehyde superplasticizers on concrete. *Cem. Concr. Res.* **1988**, *18*, 513–531. [CrossRef]
20. Ludvig, P.; Viana, T.M.; Nehme, S.G. Ultra-high performance concrete with carbon nanotubes and different types of superplasticizing admixtures: Behavior at high temperatures. *J. Build. Pathol. Rehabil.* **2026**, *11*, 109. [CrossRef]
21. Tkaczewska, E. Effect of the superplasticizer type on the properties of the fly ash blended cement. *Constr. Build. Mater.* **2014**, *70*, 388–393. [CrossRef]
22. Ahmed, S.; El-Feky, M.; Hefne, E. Naphthalene-sulfonate-based super-plasticizer and ultra-sonication effects on the dispersion of CNT in cement composites subjected to cyclic loading. *Int. J. Mod. Trends Eng. Res.* **2018**, *5*, 269–279.
23. Li, P.; Yu, Q.; Brouwers, H. Effect of PCE-type superplasticizer on early-age behaviour of ultra-high performance concrete (UHPC). *Constr. Build. Mater.* **2017**, *153*, 740–750. [CrossRef]
24. Yang, Y.; Tan, Y.; Li, Z.; Zhou, G.; Yu, X.; Xu, D.; Yong, Q.; Zhao, H.; Xie, Z. Interaction mechanisms between polycarboxylate superplasticizers and cement, and the influence of functional groups on superplasticizer performance: A review. *Polym. Bull.* **2024**, *81*, 10415–10438. [CrossRef]
25. Nitin; Chaudhary, V.; Yeshpal. Review of advanced cementitious composites using water soluble polymer based admixture. *J. Appl. Polym. Sci.* **2024**, *141*, e55430. [CrossRef]
26. Ghahsareh, F.M.; Meng, W. Cellulose Nanocrystals in Cementitious Composites: Dispersion Strategies and Enhancement Mechanisms. *J. Build. Eng.* **2025**, *112*, 113847. [CrossRef]
27. Wang, J.; Pei, D.; Lu, L.; Zhang, F.; Luo, Q.; Liu, Y.; Xing, F. Impacts of nano CSH-PCE on durability-related properties of Portland cement composites with high-volume GGBFS. *Constr. Build. Mater.* **2024**, *449*, 138547. [CrossRef]
28. Fan, Q.; Zheng, Y.; Meng, D.; Guo, Q.; Liu, Y.; Wu, H. Study on improving the performance of engineered cement-based composites by modifying binder system and polyethylene fiber/matrix interface. *Colloids Surf. Physicochem. Eng. Asp.* **2025**, *707*, 135862. [CrossRef]
29. Mao, Y.; Hu, X.; Yang, L.; Shi, C. A review on design and performance regulation of ultra-high performance concrete (UHPC). *J. Sustain.-Cem.-Based Mater.* **2024**, *14*, 1704–1725. [CrossRef]
30. Nkinamubanzi, P.C.; Mantellato, S.; Flatt, R. Superplasticizers in practice. In *Science and Technology of Concrete Admixtures*; Elsevier: Amsterdam, The Netherlands, 2016; pp. 353–377.
31. Aitcin, P.C.; Jolicoeur, C.; MacGregor, J.G. Superplasticizers: How they Work and Why They Occasionally Don't. *Concr. Int.* **1994**, *16*, 45–52.
32. Lei, L.; Plank, J. 40 Years of PCE Superplasticizers-Current State of the Art and Future Perspectives. *ce/papers* **2023**, *6*, 594–599. [CrossRef]
33. Wang, X.; Huang, X.; Duan, Z.; Lu, L.; Sheng, S.; Ye, M. Method for Preparing Dry Powder Polycarboxylate Superplasticizer. Chinese Patent CN105776937A, 20 July 2016.
34. Chandra, S.; Björnström, J. Influence of superplasticizer type and dosage on the slump loss of Portland cement mortars—Part II. *Cem. Concr. Res.* **2002**, *32*, 1613–1619. [CrossRef]
35. Liu, Y.; Song, P.; Kong, L.; Xu, L.; Li, C.; Zhou, Z.; Sun, G. Influence of retarders on the performance of slag-silica fume based ultra-high-performance geopolymer concrete. *J. Build. Eng.* **2025**, *112*, 113891. [CrossRef]

36. Alsadey, S.; Omran, A. Effect of Superplasticizers to Enhance the Properties of Concrete. *Des. Constr. Maint.* **2022**, *2*, 84–91. [CrossRef]
37. Huang, K.; Xie, J.; Wang, R.; Feng, Y.; Rao, R. Effects of the combined usage of nanomaterials and steel fibres on the workability, compressive strength, and microstructure of ultra-high performance concrete. *Nanotechnol. Rev.* **2021**, *10*, 304–317. [CrossRef]
38. Miličević, I.; Bušić, R.; Bebek, K.; Briševac, D. Influence of superplasticizer type and dosage on retention of consistency of rubberized concrete. *WIT Trans. Built Environ.* **2022**, *209*, 23–31.
39. Papayianni, I.; Tsohos, G.; Oikonomou, N.; Mavria, P. Influence of superplasticizer type and mix design parameters on the performance of them in concrete mixtures. *Cem. Concr. Compos.* **2005**, *27*, 217–222. [CrossRef]
40. El Bitouri, Y.; Azema, N. On the "Thixotropic" Behavior of Fresh Cement Pastes. *Eng* **2022**, *3*, 677–692. [CrossRef]
41. Bauchkar, S.; Chore, H. Effect of PCE superplasticizers on rheological and strength properties of high strength self-consolidating concrete. *Adv. Concr. Constr.* **2018**, *6*, 561.
42. Zhu, S.; Liu, J.; Zhang, Y.; Li, M. Study on the influence of early strength polycarboxylate superplasticizer on early performance of concrete. *J. Phys. Conf. Ser.* **2023**, *2539*, 012027. [CrossRef]
43. Cavusoglu, I. Superplasticizer Dosage Effect on Strength, Microstructure and Permeability Enhancement of Cementitious Paste Fills. *Minerals* **2024**, *14*, 1242. [CrossRef]
44. Schmidt, W.; Brouwers, H.J.H.; Kuehne, H.C.; Meng, B. Effects of the characteristics of high range water reducing agents and the water to powder ratio on rheological and setting behavior of self-consolidating concrete. *Adv. Civ. Eng. Mater.* **2015**, *3*, 1–15. [CrossRef]
45. Yu, R.; Spiesz, P.; Brouwers, H.J.H. Development of ultra-high performance fibre reinforced concrete (UHPFRC): Towards an efficient utilization of binders and fibres. *Constr. Build. Mater.* **2015**, *79*, 273–282. [CrossRef]
46. Shi, C.; Wu, Z.; Xiao, J.; Wang, D.; Huang, Z.; Fang, Z. A review on ultra high performance concrete: Part I. Raw materials and mixture design. *Constr. Build. Mater.* **2015**, *96*, 368–377. [CrossRef]
47. Tian, Y.; Yan, X.; Lu, D.; Wang, Z.; Jun, Z.; Xu, O.; Li, W. Characteristics of the cement asphalt emulsion mixture with early-age strength and flowability. *Front. Mater.* **2020**, *7*, 122. [CrossRef]
48. Abril-Fernández, M.Y.; Óscar, G.J.; Alarcon, J.J. Influence of superplasticiser additives on the properties of high-performance concrete: A systematic review. *Organ. Technol. Manag. Constr.* **2025**, *17*, 260–278. [CrossRef]
49. *ASTM C109/C109M-21*; Standard Test Method for Compressive Strength of Hydraulic Cement Mortars. ASTM International: West Conshohocken, PA, USA, 2021.
50. *ASTM C1437-20*; Standard Test Method for Flow of Hydraulic Cement Mortar. ASTM International: West Conshohocken, PA, USA, 2007.
51. *ASTM C39/C39M-14*; Standard Test Method for Compressive Strength of Cylindrical Concrete Specimens. ASTM International: West Conshohocken, PA, USA, 2014.
52. *ASTM C39/C39M-21*; Standard Test Method for Compressive Strength of Cylindrical Concrete Specimens. ASTM International: West Conshohocken, PA, USA, 2021.

Disclaimer/Publisher's Note: The statements, opinions and data contained in all publications are solely those of the individual author(s) and contributor(s) and not of MDPI and/or the editor(s). MDPI and/or the editor(s) disclaim responsibility for any injury to people or property resulting from any ideas, methods, instructions or products referred to in the content.